Nanoscale Advances

ROYAL SOCIETY OF CHEMISTRY

PAPER

View Article Online
View Journal | View Issue

Cite this: *Nanoscale Adv.*, 2024, **6**, 4180

Targeted treatment of rat AKI induced by rhabdomyolysis using BMSC derived magnetic exosomes and its mechanism†

Yuling Chen *[ab] and Shike Hou[ab]

Introduction: rhabdomyolysis (RM) is a serious syndrome. A large area of muscle injury and dissolution induces acute kidney injury (AKI), which results in a high incidence and mortality rate. Exosomes released by mesenchymal stem cells (MSCs) have been used to treat AKI induced by rhabdomyolysis and have shown regenerative effects. However, the most serious drawbacks of these methods are poor targeting and a low enrichment rate after systemic administration. *Methods*: in this study, we demonstrated that magnetic exosomes derived from bone marrow mesenchymal stem cells (BMSCs) can directly target damaged muscles rather than kidneys using an external magnetic field. *Results*: magnetic navigation exosomes reduced the dissolution of damaged muscles, greatly reduced the release of cellular contents, slowed the development of AKI. *Discussion*: in summary, our proposed method can overcome the shortcomings of poor targeting in traditional exosome therapy. Moreover, in the rhabdomyolysis-induced AKI model, we propose for the first time an exosome therapy mode that directly targets damaged muscles through magnetic navigation.

Received 22nd April 2024
Accepted 11th June 2024

DOI: 10.1039/d4na00334a

rsc.li/nanoscale-advances

1 Introduction

Trauma-induced rhabdomyolysis and Crush syndrome are the most common diseases in wars, traffic accidents and natural disasters.[1] Acute kidney injury (AKI) is caused by skeletal muscle injury and damaged muscle cells subsequently release decomposition products into the systemic circulation.[2] AKI is a common complication of rhabdomyolysis, the incidence of which is estimated to be 10–50%.[3–6]

Mesenchymal stem cells (MSCs) have been used to repair kidney injury due to their immunoregulatory and tissue repair functions.[7] Their main mechanism is mediated by paracrine signaling rather than direct differentiation.[8] MSC-derived exosomes (Exos) are extracellular vesicles (EVs, 50–150 nm) that contain various mRNAs, microRNAs and proteins derived from parental cells.[9] The treatment of AKI with extracellular vesicles has attracted widespread attention.[10–13] To date, exosomes have been used to reduce AKI-related mitochondrial DNA damage and inflammation,[14,15] promote renal tubular repair[16] and promote renal regeneration.[10] Bruno *et al.*[17] reviewed EVs derived from mesenchymal stem cells for the treatment of AKI. However, research has found that the limitations of traditional exosome therapy, particularly in terms of poor targeting, easily cleared by the mononuclear phagocytic cell system and the lack of a precise treatment mode.[18] In addition, there is currently no single and effective treatment plan (mainly *in situ* injection) to treat rhabdomyolysis induced AKI. The specific targets and related regulatory mechanisms of kidney regeneration are also unclear. To address these issues, we propose a drug therapy model that targets damaged muscles through magnetic field guided exosomes and treats AKI by improving muscle dissolution.

Superparamagnetic iron oxide nanoparticles (SPIONs) are biocompatible and safe.[19] After being absorbed by MSCs, they can ionize into Fe ions and stimulate significant upregulation of therapeutic growth factors in MSCs through signal cascade reactions. Therefore, compared with normal MSC-EVs, magnetic EVs contain more therapeutic molecules and exhibit significant therapeutic effects.[20,21] On the other hand, magnetic exosomes can achieve precise targeted delivery under the guidance of external magnets. At present, the extracellular vesicle delivery system of SPION[22] has been used to treat infarcted heart tissue,[23] ischemic stroke,[24] and skin wound healing.[25] However, so far no research has been found on the combination of magnetic particles and extracellular vesicles using magnetic navigation to repair AKI induced by rhabdomyolysis.

This study explored the protective effect and potential mechanism of magnetic exosomes derived from BMSCs in targeted therapy for glycerol-induced AKI in rats. To obtain exosomes with good targeting ability, we coincubated the SPIONs with MSCs to prepare magnetic exosomes (Exo-SPION). They reach the leg muscles of rats with the help of an external

[a]*Institute of Disaster and Emergency Medicine, Tianjin University, Tianjin, China. E-mail: chenyuling97@outlook.com*

[b]*Tianjin Key Laboratory of Disaster Medicine Technology, Tianjin, China*

† Electronic supplementary information (ESI) available. See DOI: https://doi.org/10.1039/d4na00334a

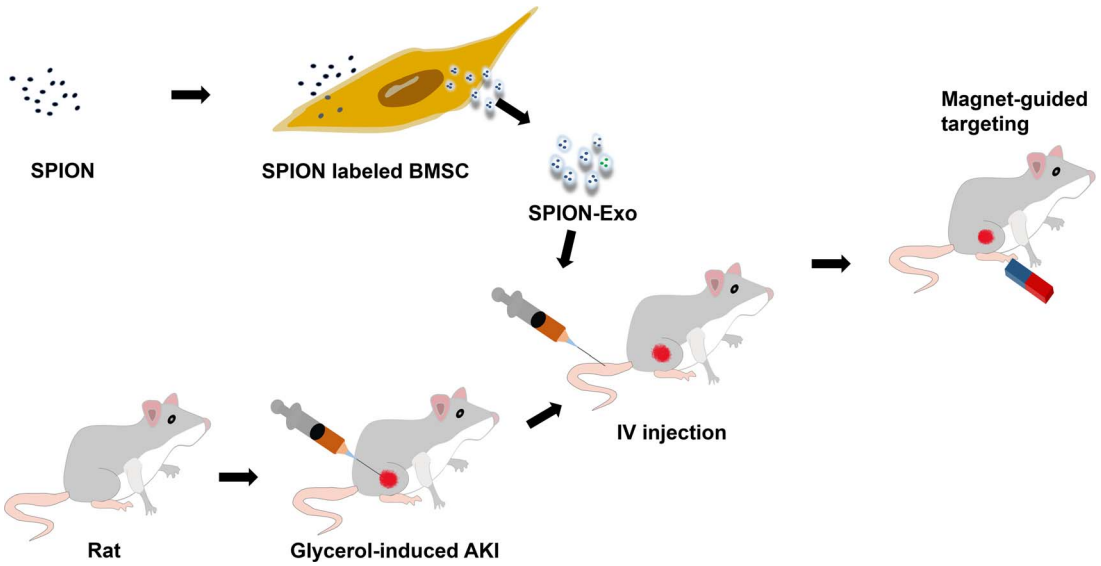

Scheme 1 Exo-SPION treatment using magnetic navigation.

magnetic field (MF), as shown in Scheme 1. Glycerol-induced skeletal myocyte lysis[26,27] was used to establish the AKI model. The magnets used in the experiment were two 20 mm (thick) × 30 mm (diameter) cylindrical magnets. This study helps to expand the treatment mode of acute kidney injury caused by muscle lysis, explore the precise targets and related regulatory mechanisms of exosome regeneration, and reveal important research significance.

2 Materials and methods

2.1 Synthesis and characterization of SPION

We synthesized SPIONs through a chemical co precipitation method. 3 g PAA (Shanghai Yuanye Biology, China, Mw = 1800) was dissolved in 100 mL of deionized water and heated to reflux. 0.52 g $FeCl_2 \cdot 4H_2O$ (Macklin, China) and 1.40 g $FeCl_3 \cdot 6H_2O$ (Macklin, China, the molar ratio of iron ion to ferrous ion is 2.45) were dissolved in HCL (2 mL, 1 M) solution in advance. Then, the mixed solution is quickly injected into the hot solution and heated at 90 °C under nitrogen flow until reflux. Add 10 mL NH_4OH (Macklin, China, 25 wt%) into the solution, stir quickly. The color of the solution quickly changes from orange to black. The solution was cooled to room temperature, and then deionized water was used for dialysis and purification. After filtration through a 0.22 μm membrane, the SPION solution was stored at room temperature until further use. The powder was also collected and stored after being freeze-dried under vacuum at −80 °C for 24 h. All the reagents were of analytical grade and were used without further purification. High purity water (Milli-Q integral) with a conductivity of 18 MΩ cm^{-1} was used to prepare all aqueous solutions. The hydrodynamic diameter of the SPIONs was measured by dynamic light scattering (DLS, Marvin, Zetasizer Nano ZS90). Moreover, the zeta potential was measured. Three measurements were made on the basis of the average digital weighted. The size and shape of the SPIONs were observed *via* transmission electron microscopy (TEM). The Fe concentration in the solution was determined *via* ICP-MS (Agilent 7700x).

2.2 Cell culture

Rat BMSCs and supporting stem cell culture media and the L6 (rat myoblast) and NRK-52e (rat renal tubular) cell lines were all purchased from OriCell (China). DMEM medium (Gibco), supplemented with 10% (v/v) fetal bovine serum (FBS), penicillin (100 U mL^{-1}) and streptomycin (100 μg mL^{-1}) were all purchased from Sparkjade (China). All cells were grown in a humidified 5% CO_2 atmosphere at 37 °C and passaged every 2 days. The generation 5–6 of BMSCs were tested.

2.3 Preparation and characterization of Exo-SPION

To evaluate the cytotoxicity of the SPIONs to BMSC and NRK-52e, we determined the Fe concentration using ICP-MS and prepared the SPIONs at 0, 6.25, 12.5, 25, 50, 100, 200, 400 μg Fe per mL in the culture medium. The time points 1 d, 3 d were set, and the activity of SPION-treated BMSC and NRK-52e was determined using a Cell Counting Kit-8 (CCK-8, Sparkjade, China) assay. Based on these results, the most suitable concentration of 25 μg Fe per mL was selected, and this concentration was used in subsequent experiments.

We inoculated 1×10^6 BMSCs in a T-75 culture bottle and added 15 mL of complete culture medium for 48 hours (cell density 80%). The medium was then changed to conditioned medium containing 25 μg Fe per mL SPION for 24 hours. The BMSCs were thoroughly washed with PBS three times to remove the free SPIONs. To visualize the internalization of SPION in BMSCs, TEM (LIBRA 120, Carl Zeiss, Germany) and Prussian blue staining (Stain according to Prussian Blue Staining Kit, Solarbio, China) were used to observe BMSC-SPION. Afterwards, the culture was continued for 48 hours in serum-free medium. The supernatant was collected and centrifuged at 1500 rpm for 15 minutes to remove dead cells and cell fragments. Afterwards, the supernatant was centrifuged at

10 000×*g* for 30 minutes and 100 000×*g* for 70 minutes. Exo-SPION was collected, resuspended in PBS, centrifuged at 100 000×*g* for 70 minutes, resuspended in PBS and stored at −80 °C. The steps in the normal exosome collection process were the same except for the conditional cultivation without SPION.

The size and quantity of Exo-SPION were determined using TEM (JEM-2100F) observation and nanoparticle tracking analysis (NTA, PSS Nicomp 380 Z3000). The specific software is ZetaView (8.04.02 SP2) for the NTA data analysis. The total protein concentrations of Exo and Exo-SPION were determined using a BCA kit for western blot protein characterization. RIPA buffer was used to lyse cells and exosomes on ice to prepare homogenate (15 μg total protein loading). The antibodies used were anti-CD81 (Cat No. 66866-1-Ig), anti-TSG-101 (Cat No. 67381-1-Ig) and anti-Alix (Cat No. 67715-1-Ig), with anti-calnexin (Cat No. 66903-1-Ig) serving as the positive control and no negative control. All the antibodies used were purchased from Proteintech Group, Inc. (China). The secondary antibodies used were goat anti-mouse IgG (H + L) HRP (1 : 5000, # EF0001, SparkJade, China), goat anti-rabbit IgG (H + L) HRP (1 : 5000, # EF0002, SparkJade, China) and enhanced chemiluminescence (ECL) reagent (Tanon, # 180–501). Finally, Tanon Gel Pro instrument was used for imprinting and detection.

2.4 Glycerol-induced AKI model

Wistar rats (male, 180–200 g, Charles River, China) were used for all the experiments. The controlled environmental parameters were 22 °C ± 1 °C and 60 ± 5% humidity, with 12 : 12 hours of light: darkness cycles. Rats were allowed to freely feed on standard feed pellets and tap water. All the experimental procedures were carried out in accordance with the Guidelines for the Care and Use of Experimental Animals approved by the National Institutes of Health of the United States and were approved by the Experimental Animal Ethics Committee of Tianjin University (No. TJUE-2023-170).

The rats were deprived of water 24 hours in advance but were not fasted. The rats were anesthetized by intraperitoneal injection of 10% Ulatan solution at dose of 0.3 mL/100 g. The experiment was conducted after the rats stopped moving. 50% glycerol solution (diluted with physiological saline) was injected into the muscles of both hind limbs of the rats at dosage of 10 mL kg^{-1}. Observing the urine of the rats turning brown indicates successful modeling. Control group (without glycerol injection, $n = 3$) and glycerol group were established. The glycerol groups were further divided into four groups ($n = 6$): the PBS group, Exo group, Exo-SPION group and Exo-SPION+MF group. After intramuscular injection of glycerol, the cells were injected into the tail vein with PBS, Exo, Exo-SPION or Exo-SPION+MF (1 μg μL^{-1} protein, 200 μL). In the Exo-SPION+MF group, two cylindrical neodymium magnets (30 × 20 mm^3, 0.32 T) were applied for 2 hours, after which the effectiveness of the targeted administration was evaluated.

2.5 *In vivo* distribution and therapeutic effects of Exo-SPION in an AKI model

Preliminary experiments were performed ($n = 3$). After 3 days of treatment, the rats were killed. The hearts, livers, spleens, lungs, kidneys and hindlimb muscles of the rats were removed and placed in 4% tissue fixative for 48 hours. The paraffin-embedded sections were stained with Prussian blue reagent (Solarbio) to observe the distribution of Exo-SPION in the rats. The slices were cultured in PB solution (5% hydrochloric acid and 5% potassium ferrocyanide) for 40 minutes and restained with nuclear fixation red for 10 minutes. Finally, the sections were rinsed with ultrapure water three times, dehydrated with ethanol, clarified with xylene, placed on cover glass and observed under an optical microscope.

Blood was drawn from the rats (formal experiment) through puncture of the ventral aorta. The collected blood was centrifuged at 3000 rpm for 15 minutes at 4 °C, and the collected serum was stored at −80 °C. The concentrations of creatine phosphokinase (CK), creatinine (Cre) and urea in the serum were subsequently detected *via* biochemical analyzer (iMagic-V7, Icubio, China). 3 test kits were obtained from Icubio.

The lactate dehydrogenase (LDH) assay kit, heme oxygenase-1 (HO-1) assay kit, total superoxide dismutase (SOD) assay kit and kidney injury molecule 1 (Kim-1) assay kit were used to measure the levels of LDH, HO-1, Kim-1 and SOD in the serum to evaluate oxidative stress and kidney injury levels (4 test kits all from Nanjing Jiancheng, China). The determination of iron content in the heart, liver, spleen, lung and kidney of rats by ICP-MS.

The lungs, left kidneys and hind limb muscles were removed and placed in 10% tissue fixative for 48 hours. The tissues were embedded in paraffin, cut into 4 μm slices and stained with HE for morphological analysis. Images were obtained using an IVIS spectral imaging system (PerkinElmer). The left kidney also underwent TUNEL staining. The results of HE staining were used to evaluate the severity of kidney injury. The final score reflects the degree of tubular formation, brush edge loss, renal tubular necrosis and dilation in 20 randomly selected fields of view (200×). The scoring criteria were as follows: 0, none; 1, ≤ 10%; 2, 11–25%; 3, 26–45%; 4, 46–75%; and 5, ≥ 76%. Another kidney sample was frozen in liquid nitrogen and stored in −80 °C freezer for western blot analysis of related protein expression. The antibodies used were as follows: GAPDH (Proteintech, Cat No. 60004-1-Ig, China), IL-10 (Cell Signaling Technology), Bcl2 (Proteintech, 68103-1-Ig, China), IL-1β (Cell Signaling Technology), caspase-3 (Cell Signaling Technology), INOS (Cell Signaling Technology).

2.6 Study on the therapeutic mechanism of Exo-SPION

BMSCs were inoculated in T75 culture flasks for 24 hours. Afterwards, the cells were divided into cell-free group (medium), BMSC group (medium) and BMSC+SPION group (medium and SPION). After 24 hours of cultivation, the cells were washed three times with PBS, after which the medium was replaced with serum-free medium. Two days later, three sets of conditioned media were collected, and the supernatant was centrifuged and stored at −80 °C.

L6/NRK-52e cells were inoculated in 6-well plates (1 × 10^5 cells per well) for 24 hours. After being stimulated for 10 minutes with H_2O_2 (200 μM) or LPS (100 ng mL^{-1}) for 24 hours,

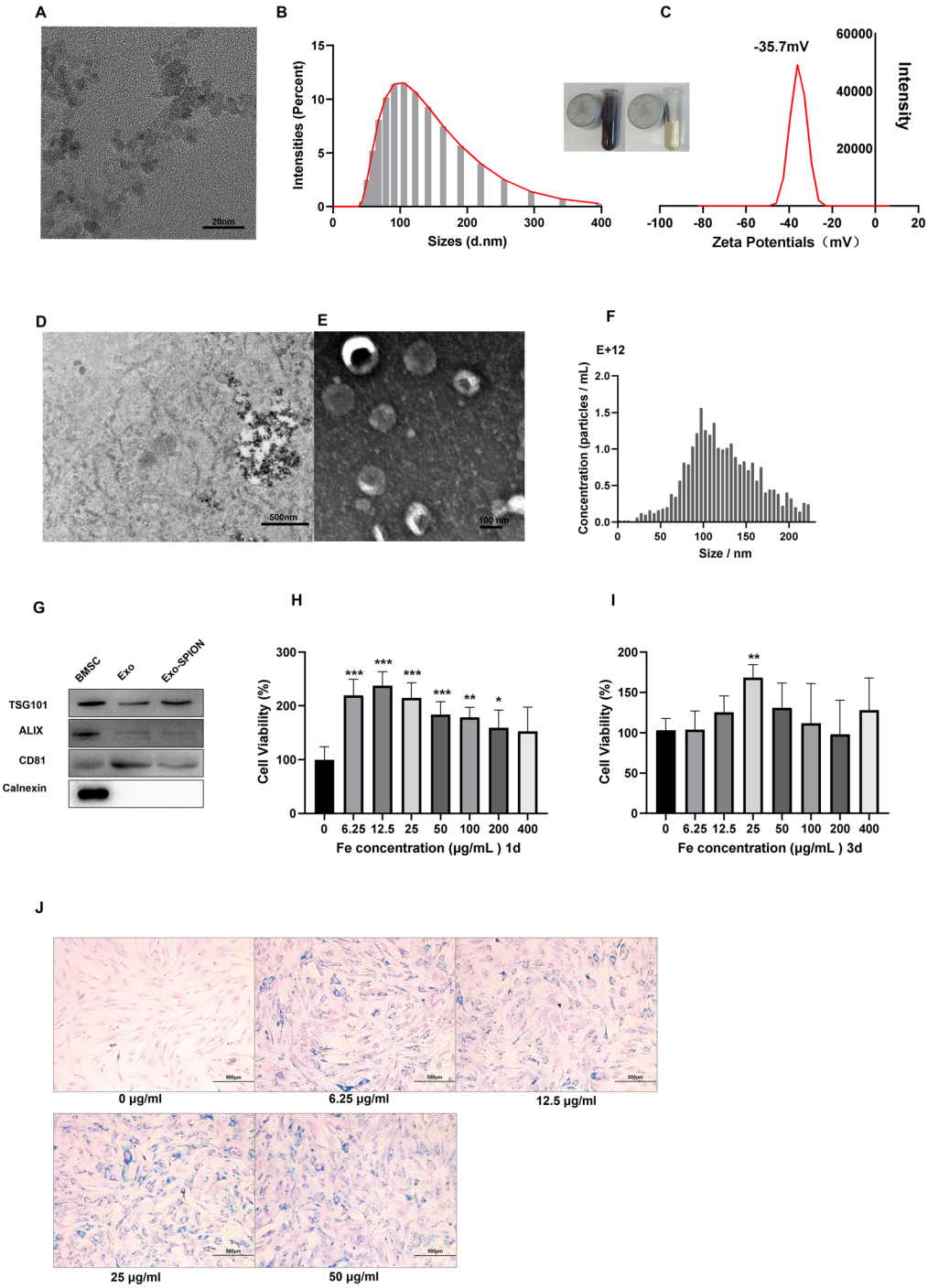

Fig. 1 Characterization of SPION and Exo-SPION. (A) Representative TEM images of SPION. Scale, 20 nm. (B) DLS was used to measure the average hydrodynamic size of the SPIONs. (C) Zeta potential of the SPIONs. (D) TEM image of BMSC-SPION showing an enlarged view of endosomes. Scale bar, 500 nm. (E) Morphology of Exo-SPION under TEM scale bars, 100 nm. (F) Representative nanoparticle tracking analysis of Exo-SPION. (G) Exo specific biomarkers (CD81, TSG101, Alix and calnexin) in Exo, Exo-SPION and BMSC whole-cell lysates were analyzed *via* western blotting. (H and I) Toxicity study of the SPION on BMSCs. CCK-8 assay was used to evaluate the proliferation of BMSCs treated with different concentrations of SPION. (J) The dose dependent uptake of SPION by BMSCs was evaluated by Prussian blue staining. Blue represents SPIONs in BMSC. Scale bar, 500 μm (*P < 0.05, **P < 0.01, ***P < 0.001 compared to 0 μg Fe per mL; n = 6).

the supernatant was replaced with the above conditioned medium, after which the cells were cultured at 37 °C for 6 hours. The cell grouping is shown in Fig. S.1.† The magnet used in the Exo-SPION+MF group was consistent with the *in vivo* experimental magnets. Finally, the cells were lysed on ice using RIPA buffer to prepare homogenates (100 μg total protein). Protein blotting was used to detect the ERK protein. ImageJ software was used to analyze the grayscale values. The

antibodies used were as follows: GAPDH (Proteintech, Cat No. 60004-1-Ig, China), p-ERK (Cell Signaling Technology), ERK (Proteintech, 11257-1-AP, China), WNT (Cell Signaling Technology), and β-catenin (Cell Signaling Technology). Finally, cell slides were made and stained with Prussian blue.

2.7 Statistical analysis

The *in vitro* and *in vivo* data are presented as the mean ± standard deviation. The *P* value was calculated using Prism 9 (GraphPad Prism software) through one-way ANOVA analysis of variance. $P < 0.05$ was considered to indicate statistical significance.

3 Results and discussion

3.1 Characterization of SPIONs and Exo-SPION

In the TEM image, we counted 20 magnetic particles (Fig. 1A) and found that the size of the Fe_3O_4 core was 7 nm. The hydrodynamic size *Z*-average of the SPIONs was 111.3 nm (Fig. 1B). The zeta potential of SPIONs was −35.7 mV (Fig. 1C). We treated BMSCs with SPION and observed their distribution within cells (Fig. 1D). Fig. 1E shows TEM image of Exo-SPION secreted by BMSCs after phagocytosis of SPION. The typical circular to elliptical vesicles shown in the image are enveloped by bilayer membrane. NTA analysis shows that the median diameter of Exo-SPION was 101.4 nm (Fig. 1F). These results are consistent with the typical size of exosomes.[28,29] Western blotting[30] confirmed the expression of the marker proteins CD81, TSG-101 and ALIX and the lack of expression of calnexin protein in Exo and Exo-SPION compared with those in BMSCs (Fig. 1G). These results further confirmed the characteristics of vesicles as exosomes. We used the CCK-8 method to evaluate the toxicity of SPION on BMSC and NRK-52e. SPION concentrations were 0, 6.25, 12.5, 25, 50, 100, 200, 400 μg Fe per mL. The time points were set to 1 d and 3 d. As shown in Fig. 1H and I, the SPIONs had almost no toxicity and has good biocompatibility with BMSCs. In addition, cell proliferation experiments showed that the activity of BMSCs depended on the concentration of SPION after co incubation for 72 hours, with peak of 25 μg Fe per mL. At this point, BMSCs exhibit significant increase in vitality. Therefore, we chose 25 μg Fe per mL SPION for the following experiments by studying the toxicity of the SPION on BMSC and

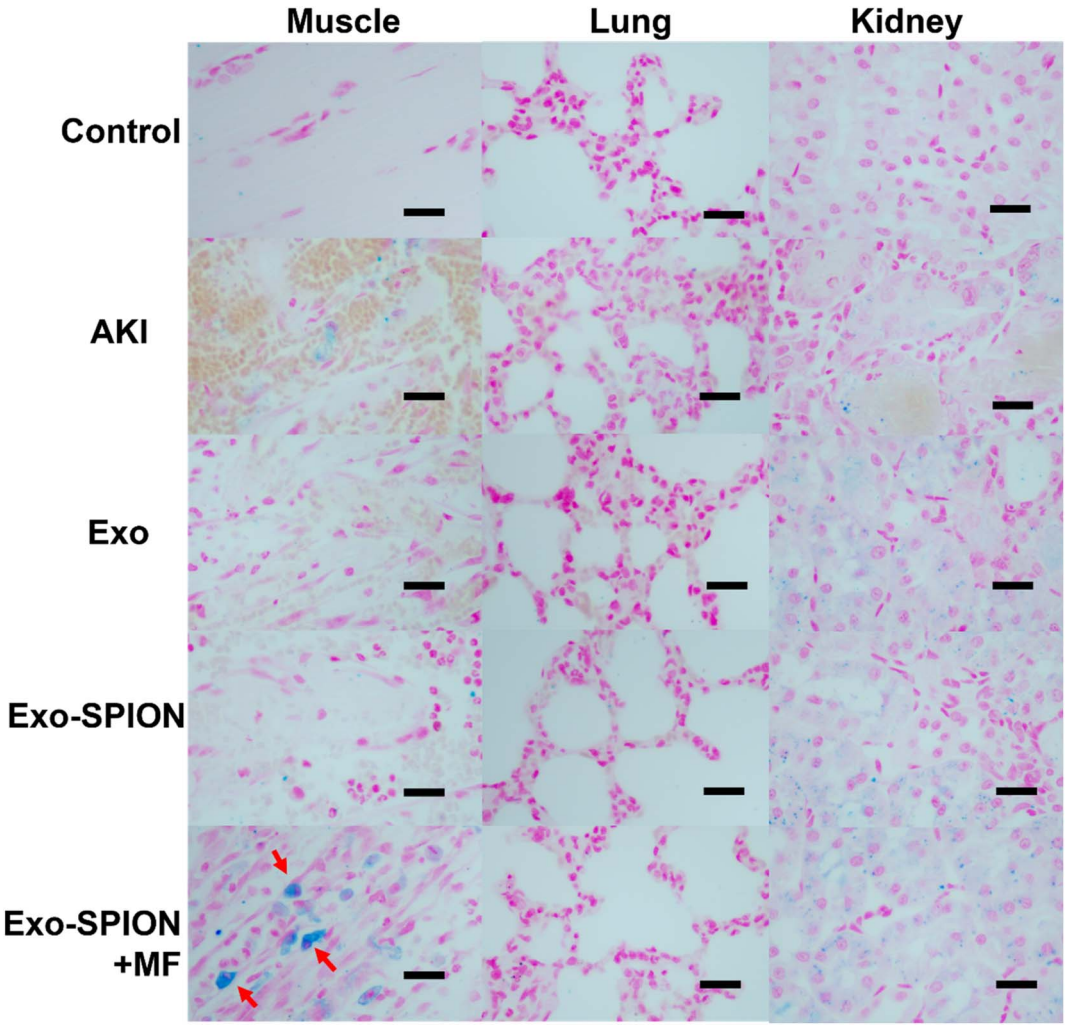

Fig. 2 Prussian blue staining of the lung, kidney and muscle 3 days after AKI was induced by glycerol. There were 6 rats in the PBS group, Exo group, Exo-SPION group and Exo-SPION+MF group. The red arrow indicates that Fe is highly enriched within the cell. Scale, 50 μm.

NRK-52e (Fig. S.2†). After two days of incubation with BMSCs, Prussian blue staining was performed on the SPIONs to analyze the labeling efficiency and cell uptake, as shown in Fig. 1J. The labeled cells showed typical blue staining, while the unlabeled cells did not show blue deposits. After Prussian blue staining, we observed that the blue particles distributed around the nucleus were phagocytosed by the cells. We found that BMSC cells treated with increasing concentrations of SPION exhibited increased proliferation and increased cell numbers under the same field of vision. No morphological differences were found between the labeled and unlabeled cells.

3.2 *In vivo* distribution of Exo-SPION in AKI model

To determine the *in vivo* localization of Exo-SPION under magnetic navigation in rats AKI injury model. 72 hours after tail vein injection, the rat hind limb muscle, heart, liver, spleen, kidney and lung tissues were removed for paraffin sectioning and then stained with Prussian blue. As shown in Fig. S.3,† we can see that the Exo-SPION+MF group exhibited significant blue staining in the damaged muscle tissue (as shown by the red arrow), while the other groups did not have blue staining in the muscles. In addition, there was almost no accumulation of Fe in the lungs, liver, spleen or heart in any of the groups. Therefore, we believe that after Exo-SPION is injected into rats, precise positioning can be achieved under the guidance of external magnets. Fig. S.4 and S.5† show the HE and Masson staining results. Based on these results, we conducted subsequent experiments.

We established control group, PBS group, Exo group, Exo-SPION group and Exo-SPION+MF group. After 3 days of tail vein administration, the kidneys, lungs and gastrocnemius muscle were removed for paraffin sectioning. The results after Prussian blue staining are shown in Fig. 2. Compared with those in normal tissues (control group), the muscles in the PBS

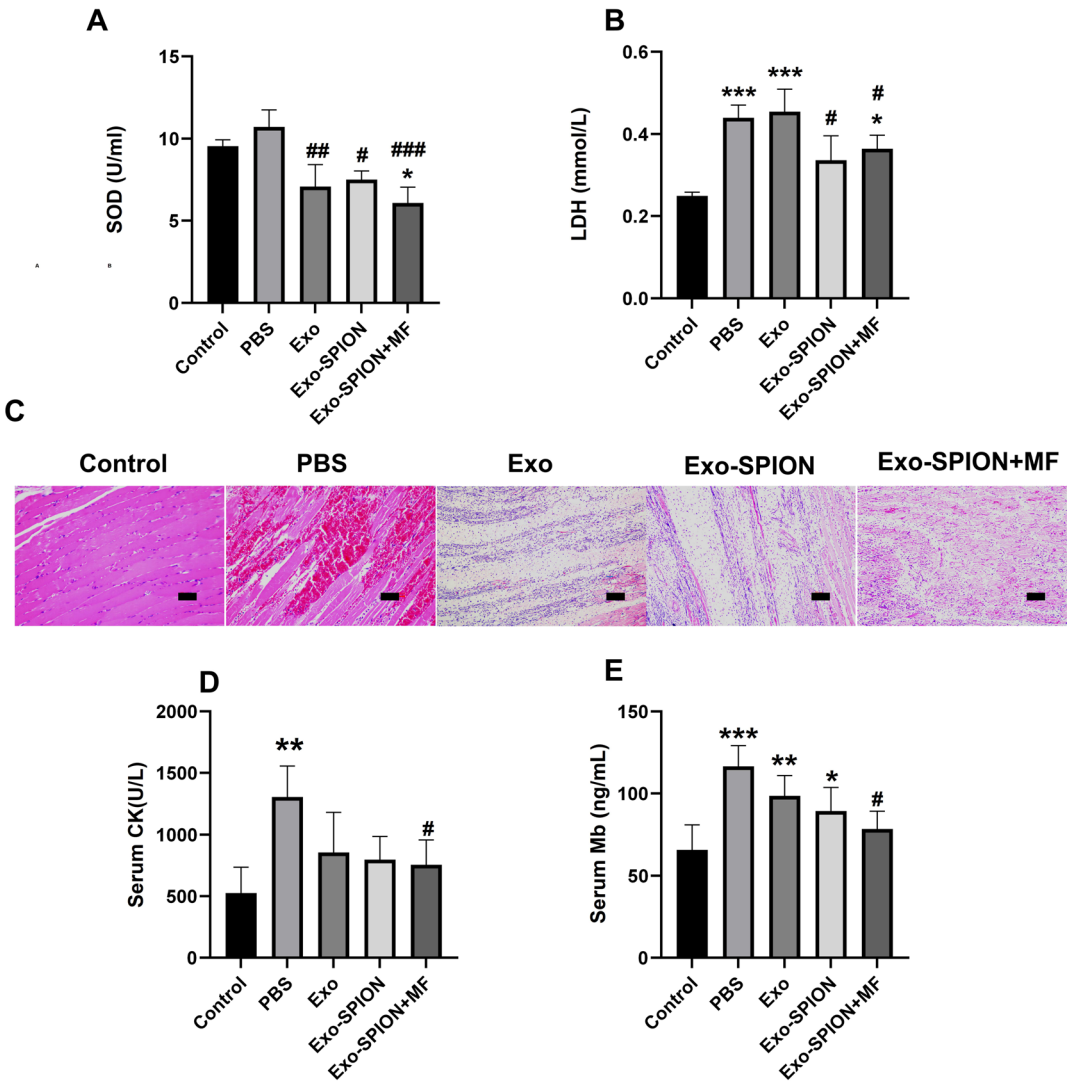

Fig. 3 Different forms of exosomes protect the muscles. There were 6 rats in the PBS group, Exo group, Exo-SPION group and Exo-SPION+MF group. Control group ($n = 3$). (A and B) After 3 days of tail vein injection, the levels of LDH and SOD in the serum of AKI rats were measured. (C) Representative micrographs of muscle tissues stained with H&E. Scale bar, 50 μm. (D and E) The serum CK and Mb levels. *$P < 0.05$, **$P < 0.01$, ***$P < 0.001$ compared to the control group. #$P < 0.05$, ##$P < 0.01$, ###$P < 0.001$ compared to the PBS group.

group exhibited obvious bleeding, degeneration, swelling, necrosis and lymphocyte infiltration. In the Exo group, Exo-SPION group and Exo-SPION+MF group, the injured gastrocnemius muscle showed fiber spacing and inflammatory cell infiltration caused by edema. In addition, we clearly observed that in muscle tissue staining, the Exo-SPION+MF group cells exhibited blue Fe deposits (indicated by the red arrow). These findings indicate that Exo-SPION is enriched in damaged muscle under the guidance of external magnets and that precise targeted drug delivery is achieved. Moreover, we also found that compared to those in the control group, the other four groups exhibited blue Fe enrichment in renal tubular epithelial cells. Surprisingly, there was also enrichment of blue Fe in the PBS and Exo groups. The same result also appears in Fig. S.3.† In this regard, we speculated that when glycerol induces muscle lysis in the legs of rats, a large amount of Fe rich myoglobin enters the blood, exits the kidney through the blood circulation, is absorbed by renal tubular epithelial cells in the kidney and is excessively enriched. Therefore, they also appear blue when dyed with Prussian blue. In addition, there was no significant impact on the alveolar walls in any of the groups. These results are consistent with the findings of Cao *et al.*,[31] who showed that Exo-SPION was preferentially enriched in the injured kidney 72 hours after injection without external magnetic guidance.

3.3 The therapeutic effect of Exo-SPION on damaged muscles in AKI model

After confirming the successful localization of Exo-SPION in injured muscles, we investigated the improvement effect of Exo-SPION in AKI rats. Three days after modeling, blood was collected from the abdominal aortas of the rats to measure the concentrations of CK, Mb, LDH and SOD in the serum. The levels of LDH and SOD in the serum of the Exo-SPION+MF group were significantly lower than those in the control group (Fig. 3A and B). These data indicate that Exo-SPION+MF alleviates glycerol induced oxidative damage in AKI rats. As shown in Fig. 3D and E, the serum levels of CK and Mb are all low. In

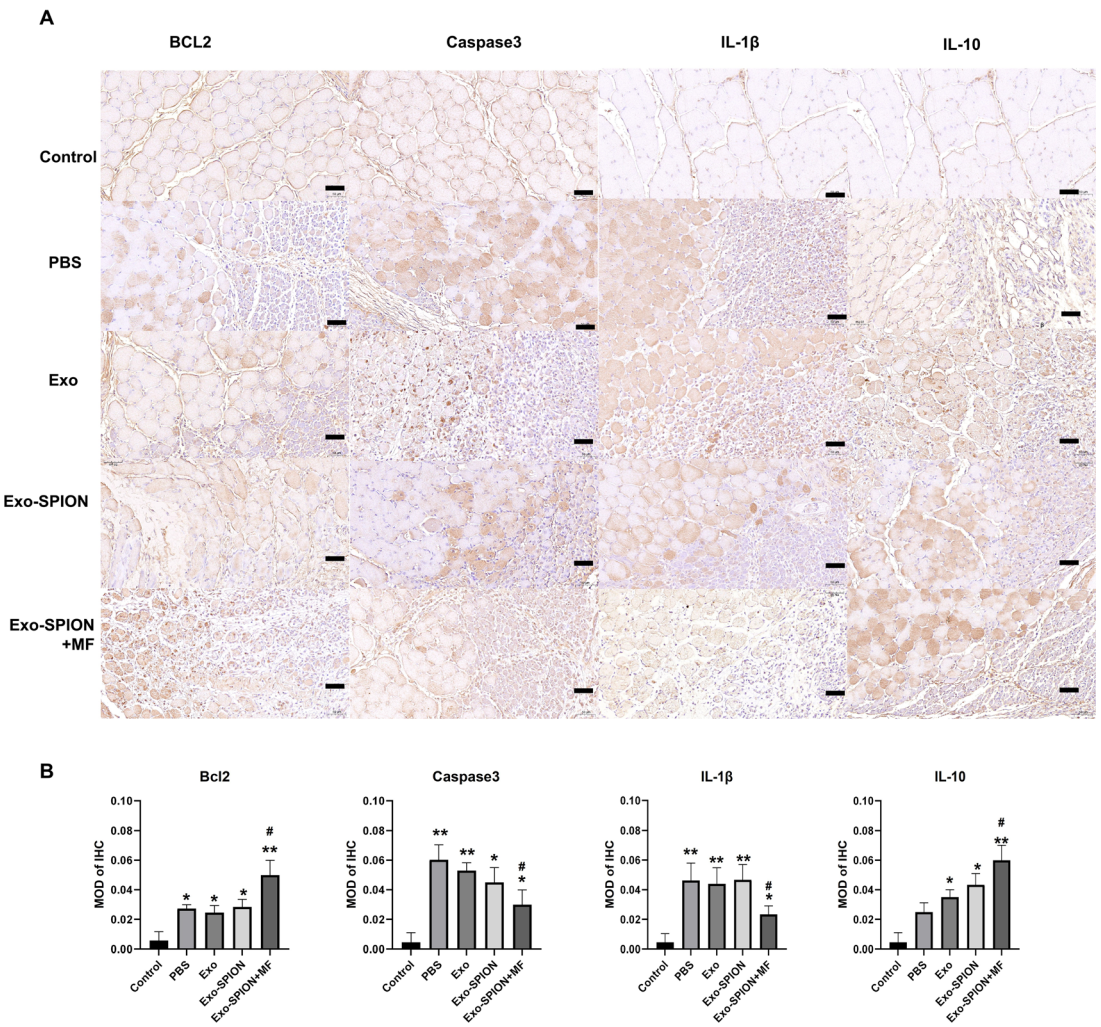

Fig. 4 The expression of Bcl2, Caspase3, IL-1β and IL-10 positive cells in the muscles of rats in each group. (A) The expression level in the muscle tissues was showed by IHC. Scale bar, 50 μm. (B) Quantitative analysis of IL-1β, IL-10, Caspase3 and Bcl2 protein expression in muscle of rats in each group. *P < 0.05, **P < 0.01 compared to the control group. #P < 0.05 compared to PBS group.

addition, the histopathological changes of rat muscles are shown in Fig. 3C. After 72 hours, the PBS group showed significant muscle fiber rupture, swelling, and infiltration of a large number of polymorphonuclear white blood cells. However, most of the muscle fibers in the Exo-SPION+MF groups did not break, and the degree of muscle fiber swelling and lymphocyte infiltration was reduced compared to the PBS group. Therefore, we believe that Exo-SPION+MF can significantly improve muscle lysis.

Immunohistochemical detection of Bcl2, Caspase3, and IL-1β and IL-10 positive cells in rat muscles were expressed (Fig. 4A), and the muscle cells in the control group were intact with lighter positive staining. More Caspase3 and IL-1β positive expression cells were observed in the PBS group. Cell counts increased and disordered cell arrangement. Compared with the PBS group, the Exo-SPION+MF group showed an increase in cell numbers, with more normal cells and positive expression cells visible. However, compared with the PBS group, the Exo-SPION+MF group showed fewer staining of Caspase3 and IL-1β positive cells, while Bcl2 and IL-10 positive cells were more stained. As shown in Fig. 4B, compared to the control group, the expression levels of Bcl2 and IL-10 proteins in the other four groups were significantly increased. Compared to the PBS group, only the Exo-SPION+MF treatment group showed significant increase in Bcl2 and IL-10 protein expression levels ($P < 0.05$). However, compared to the Control group, the other four groups of Caspase3 and IL-1β protein expression level significantly increased. Compared to the PBS group, only the Exo-SPION+MF treatment group had Caspase3 and IL-1β protein expression level significantly decreased ($P < 0.05$). Fig. S.6† show TUNEL staining of muscles. There were a small number of positive cells in the control group muscles, but the percentage of positive cells significantly increased in the PBS group. The percentage of apoptotic cells in the Exo-SPION+MF group was significantly lower than that in the PBS group ($P < 0.05$). The results indicate that the treatment with Exo-SPION+MF can significantly reduce the levels of apoptosis and inflammation in damaged muscles.

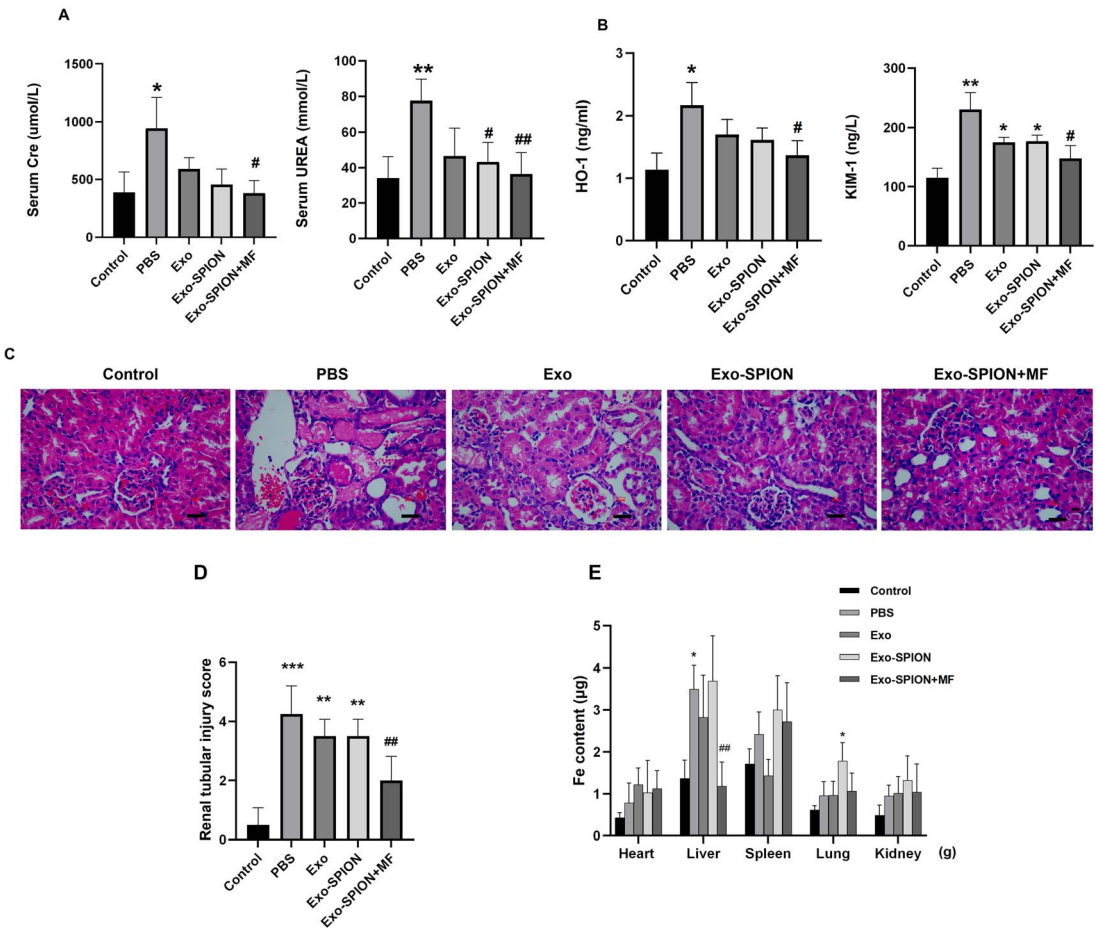

Fig. 5 Different forms of exosomes protect the kidneys. There were 6 rats in the PBS group, Exo group, Exo-SPION group and Exo-SPION+MF group. Control group ($n = 3$). (A) After 3 days of tail vein injection, the levels of Cre and UREA in the serum of AKI rats were measured. (B) The serum OH-1 and Kim-1 levels. (C) Representative micrographs of renal tissue paraffin sections stained with H&E. Treatment with Exo-SPION+MF strongly alleviated the progression of AKI. Scale bar, 50 μm. (D) Renal tubular injury score. (E) Determination of iron content in the heart, liver, spleen, lung and kidney of rats. *$P < 0.05$, **$P < 0.01$, ***$P < 0.001$ compared to the control group. #$P < 0.05$, ##$P < 0.01$ compared to the PBS group.

3.4 The therapeutic effect of Exo-SPION on damaged kidneys in AKI model

After confirming the successful localization of Exo-SPION in injured muscles, we investigated the improvement effect of Exo-SPION in AKI rats. Three days after modeling, blood was collected from the abdominal aortas of the rats to measure the concentrations of UREA and Cre in the serum. As shown in Fig. 5A, AKI injured rats exhibited significant decrease in renal function, which was reflected in the significant increase in UREA and Cre in the PBS group. The injection of Exo-SPION+MF significantly improved renal function. The serum levels of UREA and Cre are all low. The levels of OH-1 and Kim-1 in the serum of the Exo-SPION+MF group were significantly lower than those in the PBS group (Fig. 5B). These data indicate that Exo-SPION+MF alleviates glycerol induced damage to renal tubules in AKI rats. Then, on the third day after modeling, the pathological changes in the kidney tissue were analyzed through microscopy (Fig. 5C and D). The effects of different forms of exosomes on pathological changes in renal tissue were observed (×400). The renal cortex of the blank control group showed normal histology. In the PBS group, a large number of tubulin casts and necrotic areas were observed in the proximal renal tubules, necrotic cell fragments and exudates were found in the renal tubules, and myoglobin casts were observed, with normal glomerular structure. In addition, renal casting and vacuolar degeneration were observed in the Exo group and Exo-SPION group. However, after the administration of Exo-SPION+MF, AKI was significantly relieved, and smaller vacuoles were visible. Therefore, we believe that Exo-SPION+MF can significantly improve muscle lysis and slow AKI progression. The iron content in the heart, liver, spleen, lung and kidney of the rats is shown in Fig. 5E. In the PBS and Exo SPION groups, the iron concentrations in the liver and lungs were significantly increased, respectively.

Western blot analysis of the kidneys of the rats showed that the expression levels of inflammatory and apoptotic factors significantly increased within 3 days after modeling compared with those in the control group (Fig. 6A–E). The expression of IL-1β and caspase-3 decreased in the rat kidneys of the rats treated with Exo-SPION+MF. These results indicate that Exo-SPION+MF improves muscle lysis, slows down renal apoptosis and inflammation levels.

The TUNEL detection kit detects apoptotic cells in rat kidney tissue. There were a small number of TUNEL positive cells in the renal cortex area of the control group, but the number of positive cells in the PBS group significantly increased (Fig. 7). Most

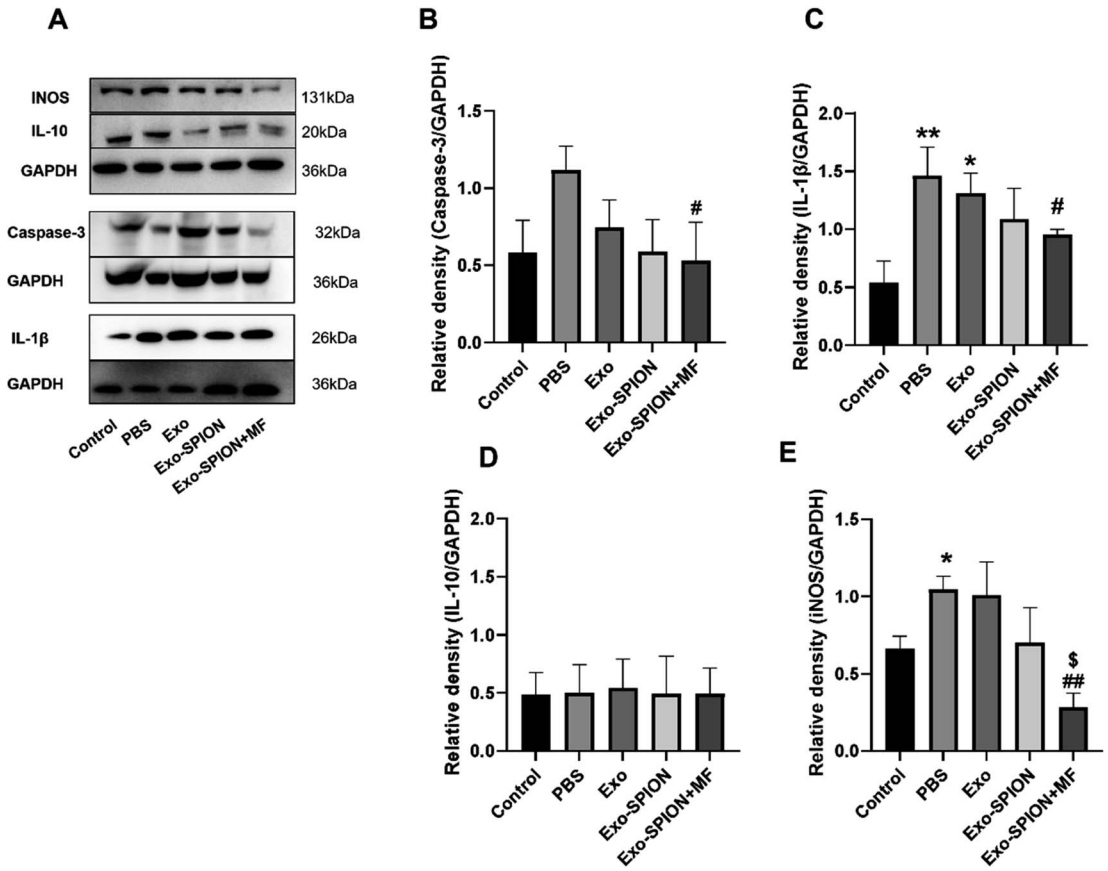

Fig. 6 Expression of proteins in the kidneys of rats. Compared with those in the control group, the inflammatory and apoptotic factors in the kidneys of the rats significantly increased within 3 days after modeling. (A) Representative images of protein imprinting in the kidneys. (B–E) Protein blotting analysis showed that treatment with exogenous Exo-SPION+MF prevents renal inflammation and apoptosis in AKI rats. *$P < 0.05$, **$P < 0.01$, ***$P < 0.001$ compared to the control group. #$P < 0.05$, ##$P < 0.01$, ###$P < 0.001$ compared to the PBS group ($n = 6$).

of them are renal tubular epithelial cells. Exo group has a large number of positive cells, followed by Exo-SPION. When using Exo-SPION+MF, fewer apoptotic cells were observed in the renal cortex (the percentage of apoptotic positive cells in Fig. S.7†). The results indicate that Exo-SPION+MF reduces cell apoptosis levels in the renal cortex by improving muscle lysis.

3.5 Therapeutic mechanism of Exo-SPION

Magnetic exosomes can be absorbed by cells *in vitro*. We applied Exo and Exo-SPION to normal L6 and NRK-52e cells and observed the cellular localization of Fe *via* Prussian blue staining. The results showed that Fe was able to directly label L6 and NRK-52e cells without changing their structure (Fig. S.8†). The Exo-SPION group cells exhibited clear blue particles uniformly distributed in the cells and surrounding areas (red arrow). These results indicate that Exo-SPION is easily internalized by L6 and NRK-52e cells.

To verify the therapeutic mechanism of magnetic exosomes *in vitro*. We treated L6 and NRK-52e cells with H_2O_2 (200 μM) and LPS (100 ng mL^{-1}). The effect of Exo-SPION on the phosphorylation level of extracellular signal-regulated kinase (ERK) was analyzed. As shown in Fig. 8, in L6 cells, the protein content of p-ERK was significantly greater in the Exo, Exo-SPION and Exo-SPION+MF groups than in the control and NO-Exo groups. These findings indicate that Exo, Exo-SPION and Exo-SPION+MF can activate the expression of p-ERK in L6 cells, which is consistent with the conclusions of Mol *et al.*,[32] Kim *et al.*,[33] Vrijsen *et al.*[34] and Ren *et al.*[35] However, Exo-SPION+MF can more effectively activate the expression of p-ERK in L6 cells compared to Exo and Exo-SPION. p-ERK activation has significant benefits for cells, it is an important mediator of growth factor induced cell proliferation and differentiation in various cell types.[36–38] Winter *et al.*[39] found that HUVECs treated with NV-IONPs exhibited significant upregulation of the phosphorylation of AKT and ERK1/2, which are involved in cell survival and migration. However, our research also revealed no significant changes in NRK-52e cells. These findings cannot indicate that Exo, Exo-SPION and Exo-SPION+MF had no effect on NRK-52e cells. According to the research results of Zhu *et al.*[40] and Zhou *et al.*,[41] extracellular vesicles activate the expression of p-ERK protein in renal tubular cells. Therefore, we speculate that the Exo, Exo-SPION and Exo-SPION+MF treatment time may be relatively short (only 6 hours in the experiment) and that ERK protein has not yet undergone changes (phosphorylation). In summary, we found that damaged L6 cells can quickly utilize Exo-SPION to upregulate the ERK signaling pathway in a short period of time, thereby regulating the expression of various repair factors.

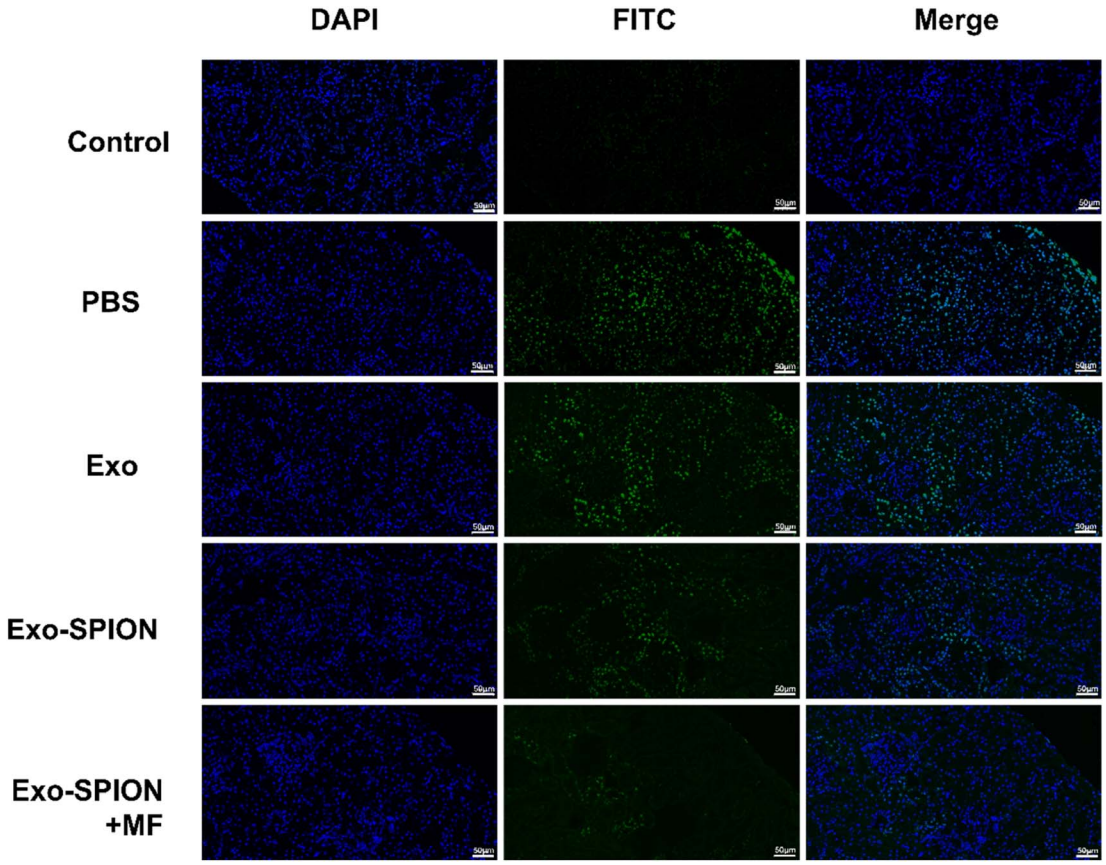

Fig. 7 TUNEL staining of apoptotic cells in renal cortex. Apoptosis positive cells appear green. Normal cells appear blue. The positive cells in the PBS group and Exo group increased significantly, followed by Exo-SPION, and the Exo-SPION+MF group decreased significantly. Scale bar, 50 μm.

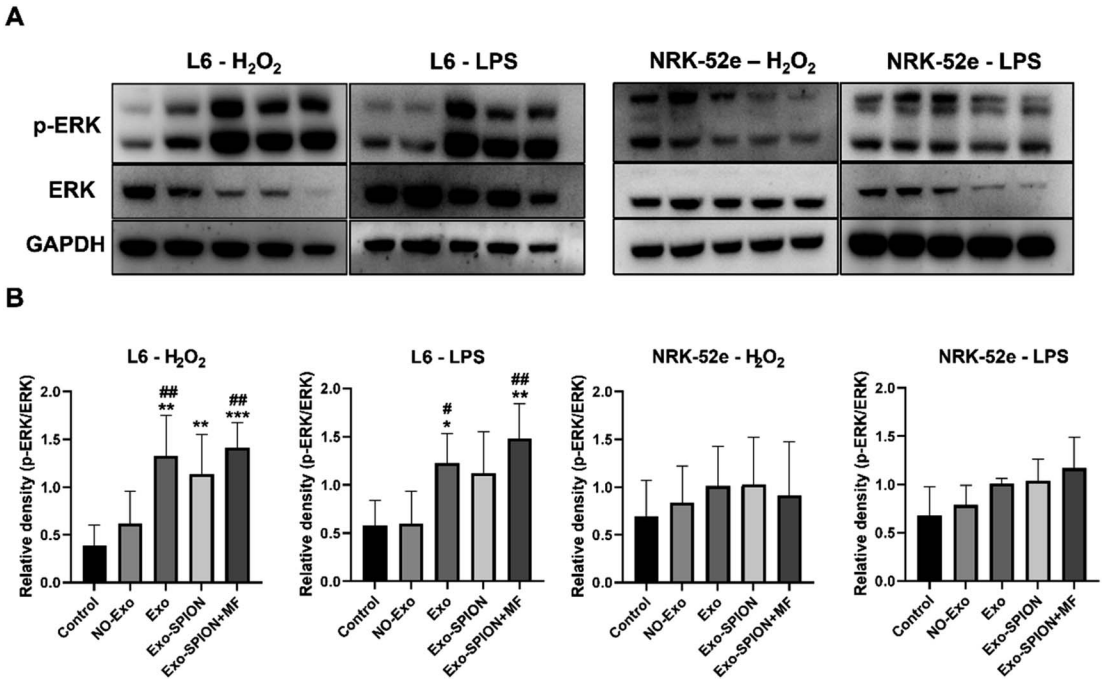

Fig. 8 The therapeutic mechanism of Exo-SPION on damaged cells. (A) The effect of different forms of Exo on the expression of p-ERK and ERK proteins was determined by western blotting. L6 and NRK-52e cells were treated with NO-Exo, Exo, Exo-SPION or Exo-SPION+MF for 6 hours. (B) Statistical map of p-ERK/ERK expression levels in L6 and NRK-52e cells. *P < 0.05, **P < 0.01, ***P < 0.001 compared to the control group; #P < 0.05, ##P < 0.01 compared to the NO-Exo group.

3.6 Treatment with Exo-SPION inhibits the WNT/β-catenin signaling pathway

To investigate the potential molecular mechanism of Exo-SPION+MF in the treatment of rhabdomyolysis, two experimental protocols were conducted *in vitro*. First, Exo, Exo-SPION and Exo-SPION+MF were applied to normal rat myoblasts and renal tubular cells. As shown in Fig. 9A, C, D, G and H, the results indicated that Exo-SPION+MF inhibited the WNT/β-catenin signaling pathway to promote damaged myoblasts healing. These results are consistent with those of Li *et al.*,[42] who suggested that BMSC-Exo inhibits WNT/β-catenin signaling to promote collagen synthesis and that this effect increases with increasing BMSC-Exo concentration.

In the NRK-52e cell results, as shown in Fig. 9B, E, F, I and J, the results indicated that Exo-SPION+MF inhibited the WNT/β-catenin signaling pathway to reduce renal tubular fibrosis. These results are consistent with the research results of Xiao *et al.*,[43] indicating that severe AKI and sustained WNT/β-catenin activation are associated. The excessive and sustained activation of the WNT/β-catenin pathway contributes to the transition from AKI to chronic kidney disease (CKD).

4 Discussion

Earthquakes, car accidents and wars caused skeletal myocyte lysis. The release of myoglobin and heme[44] by necrotic muscle cells and excess reactive oxygen species (ROS)[45] play pathogenic roles in rhabdomyolysis-induced AKI.[46] Rhabdomyolysis has been identified as prerenal factor that leads to more serious structural changes in the kidney.[47] Because there is no effective treatment, the mortality rate of AKI is still high. Here, we propose new treatment method using BMSC-Exos.

Adequate research has shown that extracellular vesicles derived from MSCs can repair AKI induced by ischemia/reperfusion.[14,31,48,49] However, a large number of studies have directly treated kidneys with drugs, and thus far, there have been no studies targeting damaged muscles. Exosomes have limited ability to target injured tissues; therefore, improving their accuracy is necessary. However, no research has been found on the improvement of AKI induced by skeletal muscle cell lysis through magnetic navigation by combining magnetic particles with exosomes. Based on these findings, we propose for the first time that magnetic exosomes released by BMSCs directly target injured muscles through magnetic navigation to improve glycerol-induced AKI.

In this study, we incorporated SPIONs into exosomes through the internalization of BMSCs without affecting their integrity or function. *In vivo*, an AKI animal model was constructed using glycerol. The precise localization of Exo-SPION *in vivo* by magnetic navigation was observed by Prussian blue staining. Interestingly, three days after Exo-SPION injection, there were no significant histopathological changes in the cellular structure of the heart, liver, spleen, lungs, and kidneys. Although iron mainly accumulates in the liver and spleen. In addition, the levels of Cre, CK and Mb in the serum of PBS group rats increased after 72 h. At the same time, the levels of Cre, CK and Mb in the serum decreased after intervention with Exo-SPION+MF. In addition, severe vascular collapse, renal tubular dilation or atrophy,

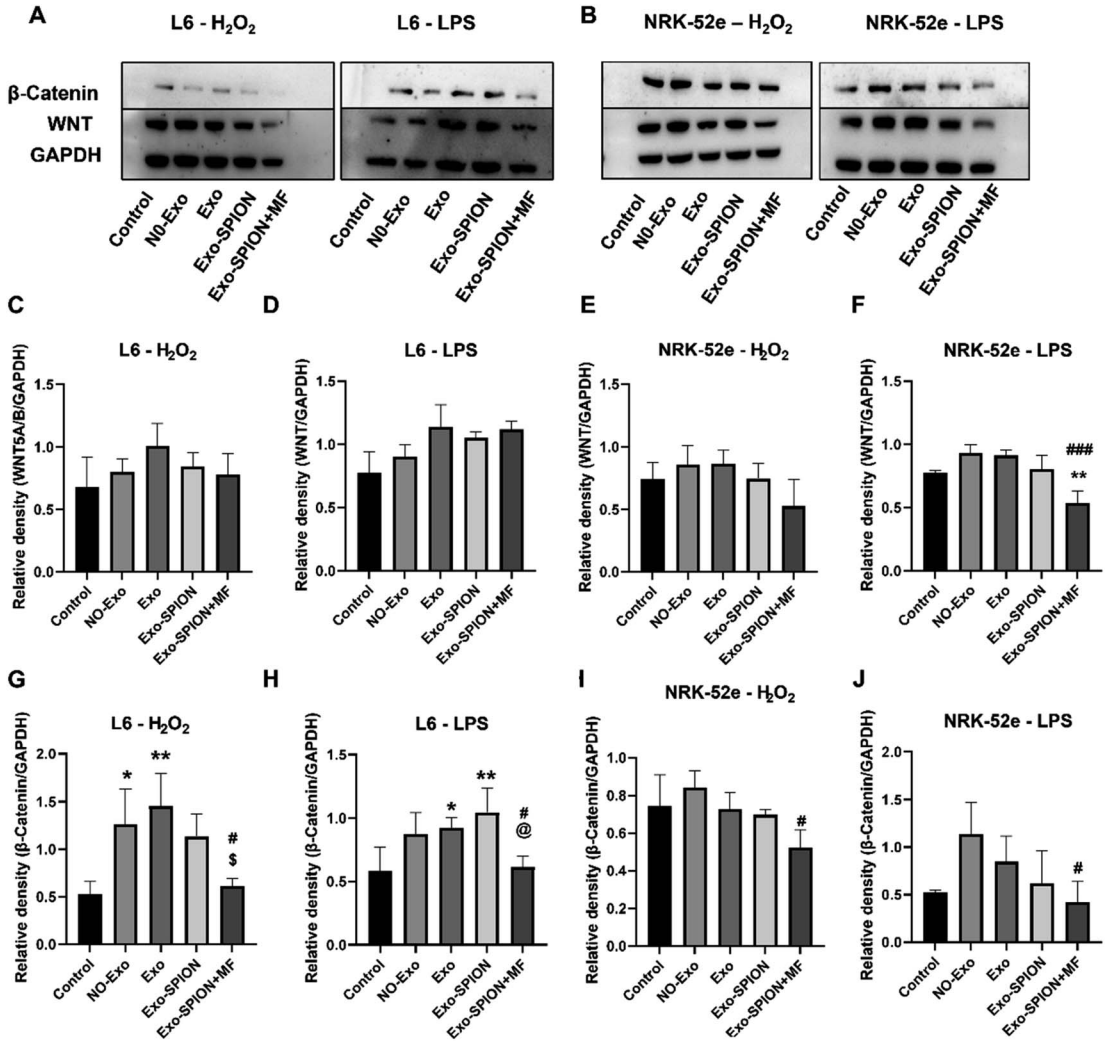

Fig. 9 Changes in the *in vitro* WNT/β-catenin signaling pathway. (A) Representative images. (B) Exo-SPION+MF inhibits WNT/β-catenin signaling pathway and reduces renal tubular cell fibrosis. (C, D, G and H) Statistical analysis of WNT and β-catenin protein expression. (E, F, I and J) Statistical analysis of WNT and β-catenin protein expression. GraphPad was used for the statistical analysis of the data. The results are expressed as the mean ± standard deviation, $^{*}P < 0.05$, $^{**}P < 0.01$ compared to the control group, $\#P < 0.05$, $\#\#\#P < 0.001$ compared to the NO-Exo group. $\$P < 0.05$ compared to the Exo group.

and inflammatory cell infiltration were observed in the renal interstitial area of PBS group rats. However, only the Exo-SPION+MF group showed significantly lower kidney damage than the PBS group. Because the source of cellular contents is only damaged muscle tissue, and their destination is systemic blood and kidneys. However, the Exo-SPION+MF group not only had serum levels of Cre, CK, and URA, but also had low levels of kidney damage. Therefore, we can speculate that the release of contents from damaged muscles in the Exo-SPION+MF group decreased, further indicating decrease in the degree of muscle damage in the Exo-SPION+MF group. Combined with *in vitro* cell experiments, the Exo-SPION+MF group enhanced the self-repair of damaged muscle cells by activating phosphorylation of ERK signals.

The glycerol induced AKI rat model is accompanied by oxidative stress. In the PBS group *in vivo*, the detection of oxidative stress products LDH and SOD significantly increased, while in the Exo-SPION+MF treatment group, they significantly decreased. The positive cells in the PBS group were higher than those in the Exo-SPION+MF group. Therefore, Exo-SPION+MF alleviated glycerol induced renal tubular oxidative damage in AKI rats. The levels of HO-1 and Kim-1 can serve as biomarkers for AKI.[50] KIM-1 and HO-1 significantly increased in the PBS group and significantly decreased in the Exo-SPION+MF treatment group. The result also indicates that Exo-SPION+MF treatment is indeed more effective compared to other treatment groups.

In addition, Exo-SPION contains a large number of therapeutic molecules[20,21] and can also be used to repair damaged cells, demonstrating significant therapeutic effects.[23–25] Exo-SPION improved the damage to L6 cells and significantly upregulated the protein expression of p-ERK. The ERK pathway is involved in oxidative stress, cell apoptosis and inflammatory responses.[51] The ERK pathway is one of the key signaling pathways related to the mitotic activation response.[52] Shabbir *et al.*[53] activated ERK1/2 signaling in human dermal fibroblasts after treatment with extracellular vesicles collected from BMSC

culture supernatant. Moreover, the ERK1/2 pathway alleviates ischemic damage by reducing cell apoptosis and oxidative stress.[54,55] The typical pathway of MAPK/ERK signaling is involved in cell proliferation and survival and plays a role in promoting the regeneration of damaged tissues.[56,57] The results of our study are consistent with those of these studies. However, Exo-SPION+MF can more effectively activate the expression of PERK in L6 cells compared to Exo and Exo-SPION. Winter *et al.*[39] found that HUVECs treated with NV-IONPs exhibited significant upregulation of the phosphorylation of AKT and ERK1/2, which are involved in cell survival and migration. In addition, ERK1/2 are necessary for repairing renal tubular epithelial cells and inhibiting fibrosis caused by renal injury,[58] and the ERK1/2 signaling pathway is related to the pathophysiology of various renal diseases, including renal I/R.[59] Lim *et al.*[60] found that Exo therapy can prevent renal injury induced by I/R *via* the ERK1/2 signaling pathway. Zhu *et al.*[40] treated human kidney 2 (HK-2) cells exposed to hypoxia/reoxygenation with hBMSC-Exos and found significant reduction in apoptosis in HK-2 cells accompanied by activation of the ERK signaling pathway. Zhou *et al.*[41] found that extracellular vesicles released by human umbilical cord mesenchymal stem cells promote significant increase in p-ERK *in vitro* and have a protective effect on cisplatin induced renal oxidative stress and apoptosis. In addition, Zhang *et al.*[61] found that ADSC-Exo treatment upregulates ERK1/2, which is also a protective mechanism mediated by extracellular vesicles against liver ischemia-reperfusion injury. However, our research also revealed no significant changes in NRK-52e cells. These findings cannot indicate that Exo, Exo-SPION and Exo-SPION+MF had no effect on NRK-52e cells. Therefore, we speculate that the Exo, Exo-SPION and Exo-SPION+MF treatment time may be relatively short (only 6 hours in the experiment) and that ERK protein has not yet undergone changes (phosphorylation). In summary, we found that damaged L6 cells can quickly utilize Exo-SPION to upregulate the ERK signaling pathway in a short period of time, thereby regulating the expression of various repair factors.

Increasing evidence confirms that activation of the WNT/β-catenin signaling pathway plays a crucial role in the proliferation phase of wound healing.[42,62] Our results indicated that Exo-SPION+MF inhibited the WNT/β-catenin signaling pathway to promote muscle tissue healing (Fig. 9A, C, D, G and H). In addition, the WNT/β-catenin pathway is briefly activated after AKI and has been identified as a protective response that minimizes cell damage by promoting renal tubular repair and regeneration.[63] The WNT/β-catenin pathway is reactivated after renal injury, participating in the occurrence and development of renal fibrosis[64,65] and playing a key role in promoting kidney repair and regeneration.[66] For example, WNT agonists improve kidney regeneration and function, while reducing inflammation and oxidative stress in the kidneys after I/R.[67] However, excessive and sustained activation of the WNT/β-catenin pathway may contribute to the transition from AKI to CKD.[43] In the process of tissue repair, WNT/β-catenin is usually suppressed and activated during organ damage and regeneration and sustained signal activation promoting fibrosis.[68–71] Sharma *et al.*[72] found that activated WNT/β-catenin signaling induces macrophage M2 polarization and promotes the progression of renal fibrosis. In the NRK-52e cell results, our results indicated that Exo-SPION + MF inhibited the WNT/β-catenin signaling pathway to reduce renal tubular fibrosis. In summary, within a short period of time (6 hours), we found that Exo-SPION+MF inhibited damaged NRK-52e cell WNT/β-catenin signal transduction significantly reduces fibrosis. Compared to L6 cells, the effect is more significant.

5 Conclusion

In conclusion, we successfully targeted the magnetic exosomes released from BMSCs directly into injured muscles through magnetic navigation, effectively improving glycerol induced acute kidney injury. *In vivo*, Exo-SPION+MF protects AKI caused by skeletal muscle cell lysis. Moreover, we explained the important role of the ERK pathway in regulating regeneration. *In vitro*, Exo-SPION+MF improved the damage to rat myoblasts and significantly upregulated the expression of the p-ERK protein, thereby regulating the expression of various repair factors. In addition, Exo-SPION+MF inhibited the WNT/β-catenin signaling pathway, promoted the healing of rat myoblasts and reduced the fibrosis of renal tubular cells. Our proposed method overcomes the shortcomings of poor targeting and the single treatment mode of traditional exosomes in treating AKI and has certain clinical significance. We hope to monitor long-term research on rats in the future and expand to other mammals.

Abbreviations

MF	Magnetic field
ADSCs	Adipose-derived stem cells
HUVECs	Human umbilical vein endothelial cells

Ethical approval

All procedures in the study were carried out in accordance with the guidelines for the care and use of experimental animals of the National Institutes of Health and were approved by the Experimental Animal Ethics Committee of Tianjin University (No. TJUE-2023-170).

Data availability

The dataset used or analyzed during the current research period can be obtained from the corresponding authors according to reasonable requirements.

Conflicts of interest

The authors declare that they have no competing interests.

Acknowledgements

This study was supported by the National Key R&D Program of China (grant number: 2022YFC3006200).

References

1 X. Bosch, E. Poch and J. M. Grau, Rhabdomyolysis and acute kidney injury, *N. Engl. J. Med.*, 2009, **361**, 62–72.
2 W. H. Bagley, H. Yang and K. H. Shah, Rhabdomyolysis, *Intern. Emerg. Med.*, 2007, **2**, 210–218.
3 G. Melli, V. Chaudhry and D. R. Cornblath, Rhabdomyolysis: an evaluation of 475 hospitalized patients, *Medicine*, 2005, **84**, 377–385.
4 Q. Chen, Y. Nan, Y. Yang, *et al.*, Nanodrugs alleviate acute kidney injury: Manipulate RONS at kidney, *Bioact. Mater.*, 2023, **22**, 141–167.
5 Z. Xiao, Q. Huang, Y. Yang, *et al.*, Emerging early diagnostic methods for acute kidney injury, *Theranostics*, 2022, **12**, 2963–2986.
6 Q. Huang, Y. Yang, T. Zhao, *et al.*, Passively-targeted mitochondrial tungsten-based nanodots for efficient acute kidney injury treatment, *Bioact. Mater.*, 2023, **21**, 381–393.
7 Y. Geng, L. Zhang, B. Fu, *et al.*, Mesenchymal stem cells ameliorate rhabdomyolysis-induced acute kidney injury via the activation of M2 macrophages, *Stem Cell Res. Ther.*, 2014, **5**, 80–101.
8 M. Gnecchi, H. He, O. D. Liang, *et al.*, Paracrine action accounts for marked protection of ischemic heart by Akt-modified mesenchymal stem cells, *Nat. Med.*, 2005, **11**, 367–368.
9 G. Raposo and W. Stoorvogel, Extracellular vesicles: exosomes, microvesicles, and friends, *J. Cell Biol.*, 2013, **200**, 373–383.
10 C. Grange, R. Skovronova, F. Marabese, *et al.*, Stem Cell-Derived Extracellular Vesicles and Kidney Regeneration, *Cells*, 2019, **8**, 1–21.
11 C. W. Yun and S. H. Lee, Potential and Therapeutic Efficacy of Cell-based Therapy Using Mesenchymal Stem Cells for Acute/chronic Kidney Disease, *Int. J. Mol. Sci.*, 2019, **20**, 32–48.
12 J. Cao, B. Wang, T. Tang, *et al.*, Three-dimensional culture of MSCs produces exosomes with improved yield and enhanced therapeutic efficacy for cisplatin-induced acute kidney injury, *Stem Cell Res. Ther.*, 2020, **11**, 206–231.
13 C. Zhang, Y. Shang, X. Chen, *et al.*, Supramolecular Nanofibers Containing Arginine-Glycine-Aspartate (RGD) Peptides Boost Therapeutic Efficacy of Extracellular Vesicles in Kidney Repair, *ACS Nano*, 2020, **14**, 12133–12147.
14 M. Zhao, S. Liu, C. Wang, *et al.*, Mesenchymal Stem Cell-Derived Extracellular Vesicles Attenuate Mitochondrial Damage and Inflammation by Stabilizing Mitochondrial DNA, *ACS Nano*, 2021, **15**, 1519–1538.
15 H. Cao, Y. Cheng, H. Gao, *et al.*, Tracking of Mesenchymal Stem Cell-Derived Extracellular Vesicles Improving Mitochondrial Function in Renal Ischemia-Reperfusion Injury, *ACS Nano*, 2020, **14**, 4014–4026.
16 J.-Y. Cao, B. Wang, T.-T. Tang, *et al.*, Exosomal miR-125b-5p deriving from mesenchymal stem cells promotes tubular repair by suppression of p53 in ischemic acute kidney injury, *Theranostics*, 2021, **11**, 5248–5266.
17 S. Bruno and G. Camussi, Exploring mesenchymal stem cell-derived extracellular vesicles in acute kidney injury, *Methods Mol. Biol.*, 2014, **1213**, 139–145.
18 T. Imai, Y. Takahashi, M. Nishikawa, *et al.*, Macrophage-dependent clearance of systemically administered B16BL6-derived exosomes from the blood circulation in mice, *J. Extracell. Vesicles*, 2015, **4**, 26238.
19 M. Auerbach, G. M. Chertow and M. Rosner, Ferumoxytol for the treatment of iron deficiency anemia, *Expert Rev. Hematol.*, 2018, **11**, 829–834.
20 J. Han, B. Kim, J.-Y. Shin, *et al.*, Iron oxide nanoparticle-mediated development of cellular gap junction crosstalk to improve mesenchymal stem cells' therapeutic efficacy for myocardial infarction, *ACS Nano*, 2015, **9**, 2805–2819.
21 H. Y. Kim, H. Kumar, M.-J. Jo, *et al.*, Therapeutic Efficacy-Potentiated and Diseased Organ-Targeting Nanovesicles Derived from Mesenchymal Stem Cells for Spinal Cord Injury Treatment, *Nano Lett.*, 2018, **18**, 4965–4975.
22 Z. Zhuo, J. Wang, Y. Luo, *et al.*, Targeted extracellular vesicle delivery systems employing superparamagnetic iron oxide nanoparticles, *Acta Biomater.*, 2021, 13–31.
23 S. Liu, X. Chen, L. Bao, *et al.*, Treatment of infarcted heart tissue via the capture and local delivery of circulating exosomes through antibody-conjugated magnetic nanoparticles, *Nat. Biomed. Eng.*, 2020, **4**, 1063–1075.
24 H. Y. Kim, T. J. Kim, L. Kang, *et al.*, Mesenchymal stem cell-derived magnetic extracellular nanovesicles for targeting and treatment of ischemic stroke, *Biomaterials*, 2020, **243**, 119942–119951.
25 X. Li, Y. Wa Ng, L. Shi, *et al.*, Magnetic targeting enhances the cutaneous wound healing effects of human mesenchymal stem cell-derived iron oxide exosomes, *J. Nanobiotechnol.*, 2020, **18**, 1–25.
26 J. Wu, X. Pan, H. Fu, *et al.*, Effect of curcumin on glycerol-induced acute kidney injury in rats, *Sci. Rep.*, 2017, **7**, 10114–10135.
27 R. A. Siddiqui, S. U. Simjee, N. Kabir, *et al.*, N-(2-hydroxyphenyl)acetamide and its gold nanoparticle conjugation prevent glycerol-induced acute kidney injury by attenuating inflammation and oxidative injury in mice, *Mol. Cell. Biochem.*, 2019, **450**, 43–52.
28 M. Mathieu, L. Martin-Jaular, G. Lavieu, *et al.*, Specificities of secretion and uptake of exosomes and other extracellular vesicles for cell-to-cell communication, *Nat. Cell Biol.*, 2019, **21**, 9–17.
29 S. Kamerkar, V. S. LeBleu, H. Sugimoto, *et al.*, Exosomes facilitate therapeutic targeting of oncogenic KRAS in pancreatic cancer, *Nature*, 2017, **546**, 498–503.
30 C. Théry, S. Amigorena, G. Raposo, *et al.*, Isolation and characterization of exosomes from cell culture supernatants and biological fluids, *Curr. Protoc. Cell Biol.*, 2006, DOI: 10.1002/0471143030.cb0322s30.
31 H. Cao, Y. Cheng, H. Gao, *et al.*, In Vivo Tracking of Mesenchymal Stem Cell-Derived Extracellular Vesicles Improving Mitochondrial Function in Renal Ischemia-Reperfusion Injury, *ACS Nano*, 2020, **14**, 4014–4026.

32 E. A. Mol, M.-J. Goumans, P. A. Doevendans, *et al.*, Higher functionality of extracellular vesicles isolated using size-exclusion chromatography compared to ultracentrifugation, *Nanomedicine*, 2017, **13**, 2061–2065.
33 M.-O. Kim, H. Jung, S.-C. Kim, *et al.*, Electromagnetic fields and nanomagnetic particles increase the osteogenic differentiation of human bone marrow-derived mesenchymal stem cells, *Int. J. Mol. Med.*, 2015, **35**, 153–160.
34 K. R. Vrijsen, J. A. Maring, S. A. J. Chamuleau, *et al.*, Exosomes from Cardiomyocyte Progenitor Cells and Mesenchymal Stem Cells Stimulate Angiogenesis Via EMMPRIN, *Adv. Healthcare Mater.*, 2016, **5**, 2555–2565.
35 S. Ren, J. Chen, D. Duscher, *et al.*, Microvesicles from human adipose stem cells promote wound healing by optimizing cellular functions via AKT and ERK signaling pathways, *Stem Cell Res. Ther.*, 2019, **10**, 47.
36 C. F. Lai, L. Chaudhary, A. Fausto, *et al.*, Erk is essential for growth, differentiation, integrin expression, and cell function in human osteoblastic cells, *J. Biol. Chem.*, 2001, **276**, 14443–14450.
37 N. Azuma, S. A. Duzgun, M. Ikeda, *et al.*, Endothelial cell response to different mechanical forces, *J. Vasc. Surg.*, 2000, **32**, 789–794.
38 A. D. Oldenhof, O. P. Shynlova, M. Liu, *et al.*, Mitogen-activated protein kinases mediate stretch-induced c-fos mRNA expression in myometrial smooth muscle cells, *Am. J. Physiol.: Cell Physiol.*, 2002, **283**, C1530–C1539.
39 J. N. Winter, L. S. Jefferson and S. R. Kimball, ERK and Akt signaling pathways function through parallel mechanisms to promote mTORC1 signaling, *Am. J. Physiol.: Cell Physiol.*, 2011, **300**, C1172–C1180.
40 G. Zhu, L. Pei, F. Lin, *et al.*, Exosomes from human-bone-marrow-derived mesenchymal stem cells protect against renal ischemia/reperfusion injury via transferring miR-199a-3p, *J. Cell. Physiol.*, 2019, **234**, 23736–23749.
41 Y. Zhou, H. Xu, W. Xu, *et al.*, Exosomes released by human umbilical cord mesenchymal stem cells protect against cisplatin-induced renal oxidative stress and apoptosis in vivo and in vitro, *Stem Cell Res. Ther.*, 2013, **4**, 34–52.
42 C. Li, Y. An, Y. Sun, *et al.*, Adipose Mesenchymal Stem Cell-Derived Exosomes Promote Wound Healing Through the WNT/β-catenin Signaling Pathway in Dermal Fibroblasts, *Stem Cell Rev. Rep.*, 2022, **18**, 2059–2073.
43 L. Xiao, D. Zhou, R. J. Tan, *et al.*, Sustained Activation of Wnt/β-Catenin Signaling Drives AKI to CKD Progression, *J. Am. Soc. Nephrol.*, 2016, **27**, 1727–1740.
44 O. Boutaud, K. P. Moore, B. J. Reeder, *et al.*, Acetaminophen inhibits hemoprotein-catalyzed lipid peroxidation and attenuates rhabdomyolysis-induced renal failure, *Proc. Natl. Acad. Sci. U. S. A.*, 2010, **107**, 2699–2704.
45 R. A. Zager, Combined mannitol and deferoxamine therapy for myohemoglobinuric renal injury and oxidant tubular stress. Mechanistic and therapeutic implications, *J. Clin. Invest.*, 1992, **90**, 711–719.
46 M.-H. Zhang, Rhabdomyolosis and its pathogenesis, *World J. Emerg. Med.*, 2012, **3**, 11–15.
47 M. A. Tienda-Vázquez, Z. P. Morreeuw, J. E. Sosa-Hernández, *et al.*, Nephroprotective Plants: A Review on the Use in Pre-Renal and Post-Renal Diseases, *Plants*, 2022, **11**, 1–27.
48 M. Ullah, D. D. Liu, S. Rai, *et al.*, Pulsed focused ultrasound enhances the therapeutic effect of mesenchymal stromal cell-derived extracellular vesicles in acute kidney injury, *Stem Cell Res. Ther.*, 2020, **11**, 398.
49 X. Geng, Q. Hong, W. Wang, *et al.*, Biological Membrane-Packed Mesenchymal Stem Cells Treat Acute Kidney Disease by Ameliorating Mitochondrial-Related Apoptosis, *Sci. Rep.*, 2017, **7**, 41136–41143.
50 R. A. Zager, A. C. M. Johnson and K. Becker, Plasma and urinary heme oxygenase-1 in AKI, *J. Am. Soc. Nephrol.*, 2012, **23**, 1048–1057.
51 S.-M. Yu and S.-J. Kim, The thymoquinone-induced production of reactive oxygen species promotes dedifferentiation through the ERK pathway and inflammation through the p38 and PI3K pathways in rabbit articular chondrocytes, *Int. J. Mol. Med.*, 2015, **35**, 325–332.
52 L. Chang and M. Karin, Mammalian MAP kinase signalling cascades, *Nature*, 2001, **410**, 37–40.
53 A. Shabbir, A. Cox, L. Rodriguez-Menocal, *et al.*, Mesenchymal Stem Cell Exosomes Induce Proliferation and Migration of Normal and Chronic Wound Fibroblasts, and Enhance Angiogenesis In Vitro, *Stem Cells Dev.*, 2015, **24**, 1635–1647.
54 D. E. Choi, J. Y. Jeong, H. Choi, *et al.*, ERK phosphorylation plays an important role in the protection afforded by hypothermia against renal ischemia-reperfusion injury, *Surgery*, 2017, **161**, 444–452.
55 Y. Yan, G. Li, X. Tian, *et al.*, Ischemic preconditioning increases GSK-3β/β-catenin levels and ameliorates liver ischemia/reperfusion injury in rats, *Int. J. Mol. Med.*, 2015, **35**, 1625–1632.
56 W. Zhang and H. T. Liu, MAPK signal pathways in the regulation of cell proliferation in mammalian cells, *Cell Res.*, 2002, **12**, 9–18.
57 B. D. Manning and A. Toker, AKT/PKB Signaling: Navigating the Network, *Cell*, 2017, **169**, 381–405.
58 H.-S. Jang, S. J. Han, J. I. Kim, *et al.*, Activation of ERK accelerates repair of renal tubular epithelial cells, whereas it inhibits progression of fibrosis following ischemia/reperfusion injury, *Biochim. Biophys. Acta*, 2013, **1832**, 1998–2008.
59 S. Kumar, D. A. Allen, J. E. Kieswich, *et al.*, Dexamethasone ameliorates renal ischemia-reperfusion injury, *J. Am. Soc. Nephrol.*, 2009, **20**, 2412–2425.
60 S. W. Lim, K. W. Kim, B. M. Kim, *et al.*, Alleviation of renal ischemia/reperfusion injury by exosomes from induced pluripotent stem cell-derived mesenchymal stem cells, *Korean J. Intern. Med.*, 2022, **37**, 411–424.
61 Y. Zhang, Y. Li, Q. Wang, *et al.*, Attenuation of hepatic ischemia-reperfusion injury by adipose stem cell-derived exosome treatment via ERK1/2 and GSK-3β signaling pathways, *Int. J. Mol. Med.*, 2022, **49**, 1–12.

62 Y. Mi, L. Zhong, S. Lu, *et al.*, Quercetin promotes cutaneous wound healing in mice through Wnt/β-catenin signaling pathway, *J. Ethnopharmacol.*, 2022, **290**, 115066–115089.
63 H. Li, J. C. K. Leung, W. H. Yiu, *et al.*, Tubular β-catenin alleviates mitochondrial dysfunction and cell death in acute kidney injury, *Cell Death Dis.*, 2022, **13**, 1061–1093.
64 T. Kawakami, S. Ren and J. S. Duffield, Wnt signalling in kidney diseases: dual roles in renal injury and repair, *J. Pathol.*, 2013, **229**, 221–231.
65 R. J. Tan, D. Zhou, L. Zhou, *et al.*, Wnt/β-catenin signaling and kidney fibrosis, *Kidney Int. Suppl.*, 2014, **4**, 84–90.
66 D. Zhou, Y. Li, L. Lin, *et al.*, Tubule-specific ablation of endogenous β-catenin aggravates acute kidney injury in mice, *Kidney Int.*, 2012, **82**, 537–547.
67 M. Kuncewitch, W.-L. Yang, L. Corbo, *et al.*, WNT Agonist Decreases Tissue Damage and Improves Renal Function After Ischemia-Reperfusion, *Shock*, 2015, **43**, 268–275.
68 L. Zhou, Y. Li, S. Hao, *et al.*, Multiple genes of the renin-angiotensin system are novel targets of Wnt/β-catenin signaling, *J. Am. Soc. Nephrol.*, 2015, **26**, 107–120.
69 Y. Zhao, C. Wang, X. Hong, *et al.*, Wnt/β-catenin signaling mediates both heart and kidney injury in type 2 cardiorenal syndrome, *Kidney Int.*, 2019, **95**, 815–829.
70 Y. Liu, New insights into epithelial-mesenchymal transition in kidney fibrosis, *J. Am. Soc. Nephrol.*, 2010, **21**, 212–222.
71 S. J. Schunk, J. Floege, D. Fliser, *et al.*, WNT-β-catenin signalling – a versatile player in kidney injury and repair, *Nat. Rev. Nephrol.*, 2021, **17**, 172–184.
72 A. Sharma, W.-L. Yang, M. Ochani, *et al.*, Mitigation of sepsis-induced inflammatory responses and organ injury through targeting Wnt/β-catenin signaling, *Sci. Rep.*, 2017, **7**, 9235–9251.